Optical Imaging of Light-Induced Thermopower in Semiconductors

François Gibelli,[1,2] Laurent Lombez,[1,2,3] Jean Rodière,[1] and Jean-François Guillemoles[1,2,3]
[1]*Institute of Research and Development of Photovoltaic Energy IRDEP (CNRS-ENSCP-EDF), UMR 7174, 6 quai Watier, 78401 Chatou, France*
[2]*NextPV, International Associate Laboratory (LIA), 4-6-1 Komaba, Meguro-ku, Tokyo 153-8904, Japan*
[3]*Ile-de-France Photovoltaic Institute (IPVF), 8, rue de la Renaissance, 92160 Antony, France*
(Received 30 September 2015; revised manuscript received 14 December 2015; published 16 February 2016)

The traditional measurement of the thermoelectric Seebeck coefficient gives a global value for a given material. This method requires heating and electrical contacts. Here, we report a local optical measurement of carrier populations which are not in thermal equilibrium with the lattice of the material. This contactless method enables access to the local gradients of the two fundamental thermodynamical properties, namely the temperature and the electrochemical potential. Therefore, we can determine the Seebeck coefficient related to the light-induced thermoelectric properties of the material. Moreover, we demonstrate the linear relationship between voltage and temperature gradients at a micrometer scale.

DOI: 10.1103/PhysRevApplied.5.024005

I. INTRODUCTION

The thermoelectric effect was discovered in 1821 by Seebeck [1] by heating metals and observing a voltage across the sample. Various techniques for measuring Seebeck coefficients in semiconducting materials have been developed for probing high-temperature conditions [2,3], high resistivity [4], thermopower in molecules [5], the organic semiconductor [6], and for measuring simultaneously the Seebeck coefficient and thermal conductivity [7]. These different techniques are very useful not only because each one addresses a specific scientific field, but also because the Seebeck coefficient can be related to other material properties influencing the electrochemical potentials [8–11].

Moreover, measurements of thermopower in light-sensitive semiconducting materials have been done under different light intensities, exhibiting thereby the variation of the Seebeck coefficient with the illumination. This so-called photo-Seebeck effect was first described by Tauc in 1955 [12]. Many materials such as lead oxide [13], zinc oxide [14], lead chromium oxide [15], silicon [16], cadmium sulfide [17,18], carbon nanotubes [19,20], molybdenum sulfide [21], graphene [22], and gallium arsenide [23] have been probed.

These classical measurements of Seebeck and photo-Seebeck effects suffer from electrical artifacts and rely on thermocouples with known materials [2].

Here, we report a thermopower analysis obtained without directly heating the lattice of the semiconducting material. This is due to the presence of carriers having an excess of kinetic energy [24] in the material thanks to the low thermalization factor with the lattice [25]. The generation of hot carriers is possible in special designed structures reducing the electron-phonon interactions [26]—often multi-quantum-well structures as shown here—or by using high-incident photon fluxes [24,27].

This method involves a light-induced thermopower by illuminating the semiconducting material with a laser beam. The generated hot-carrier electron-hole pairs recombine radiatively and this photoemitted photon flux is recorded as a photoluminescence spectrum. Therefore, this technique is totally contactless in comparison to the techniques previously mentioned and gets rid of uncertainties linked to the electrical measurement. Moreover, it enables us to study the carrier properties decoupled from the thermal gradient in the lattice, which remains at an ambient temperature locally and globally during the measurements.

II. SETUP AND SAMPLE

In photoluminescence measurements, an incident light generates electron-hole pairs in the material, and the radiative recombination is recorded as a photoluminescence spectrum, which obeys the generalized Planck's law [28,29].

$$\phi_{\mathrm{em}}(E) = DE^2A(E)\left[\exp\left(\frac{E}{k_BT_H} - \frac{\mu_\gamma}{k_BT_H}\right) - 1\right]^{-1}, \quad (1)$$

where $\phi_{\mathrm{em}}(E)$ is the absolutely calibrated photoemitted photon flux at the energy E of the emitted photon, $A(E)$ the absorption of the material that we experimentally measure with a spectrophotometer, D a constant, and k_B the Boltzmann constant.

This last expression can be linearly fitted as a function of the photon energy E and gives directly the temperature T_H of the carriers as the slope, $-1/(k_BT_H)$, and the electrochemical potential difference between the electrons and the holes that recombine μ_γ as the intercept $\mu_\gamma/(k_BT_H)$. T_H is

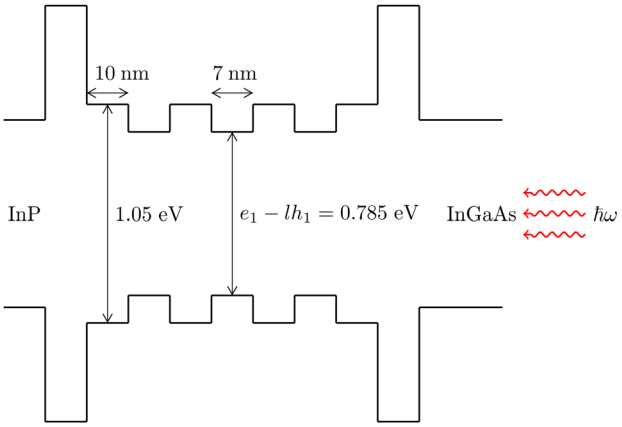

FIG. 1. Structure of the studied sample: barriers of $In_{0.8}Ga_{0.2}As_{0.44}P_{0.56}$ and wells of $In_{0.78}Ga_{0.22}As_{0.81}P_{0.19}$. This strain-balanced sample is grown by molecular beam epitaxy.

the effective temperature, representative of the electron-hole plasma temperature: electrons and holes are considered to be at this temperature T_H. The lattice of the material remains cold at ambient temperature; this method is applicable to a nonhomogeneous heated lattice too [30–32].

Spectrally resolved photoluminescence images have been measured with a hyperspectral imaging setup, with a spatial resolution down to the micrometer and spectrally calibrated between 600 and 1700 nm with a resolution of 2 nm. The excitation wavelength is 980 nm (1.26 eV), so carriers are mainly generated in the barrier energy region. Thereby, spatial variations and the influence of the considered location according to the center of the spot of the incident light in the case of a punctual illumination can be investigated.

Photoluminescence is a well-known technique for quasi-Fermi-level splitting and temperature investigations in semiconducting materials. The quasi-Fermi-level splitting is by definition the electrochemical potential difference between electron and hole carriers. As an electrochemical potential difference is related to the potential from which electrical work can be obtained, it can be identified as the internal voltage of the material [33] and can be further used for Seebeck coefficient calculations.

Multi-quantum-well materials have challenged the measurement of in-plane [34] and cross-plane [35–37] Seebeck coefficients or superlattices [38]. Here, we report measurements of the ambipolar Seebeck coefficient in the plane of the wells, but the same method could be used for the cross-plane Seebeck coefficient if there were luminescence emission coming from the barrier energy region. The sample studied here is an intrinsic quantum-well structure of InGaAsP alloy. The global structure is shown Fig. 1.

III. METHOD

The sample is probed with a fibered continuous-wave monomode laser emitting at 980 nm (1.26 eV), so the light is absorbed by both the wells and the barriers. The circular spot on the sample's surface has a radius of 8.87 μm, and the corresponding area is 2.473×10^{-10} m^2. The light emitted by the semiconducting material goes through the hyperspectral device (Photon etc.) and the data are recorded with a Xenics CCD camera [39]. Calibration procedures of the whole system are described in Ref. [33]. All experiments are done at room temperature. Sixteen data sets have been recorded at 16 different incident photon fluxes spread according to a logarithmic scale.

After converting these Cartesian maps into polar coordinates, the electrochemical potential and temperature gradients are calculated as differences between the considered pixel r on the radial coordinate, and the nearest neighbor located at $r+1$. Indeed, as the spot is circular, there is no variation of these quantities on the angular coordinates. This work is done in an area close to the incident laser beam to have noticeable variations of each quantity. The plot of this spatial electrochemical gradient against that of the temperature, shown Fig. 3(a), exhibits a linear relationship:

$$\mu_{\gamma,r+1} - \mu_{\gamma,r} = a(T_{H,r+1} - T_{H,r}) + b. \tag{2}$$

The slope a of the linear fit of this last expression gives the Seebeck coefficient α of the material, as

$$a = \frac{\mu_{\gamma,r+1} - \mu_{\gamma,r}}{T_{H,r+1} - T_{H,r}} \Leftrightarrow \alpha = \frac{\overrightarrow{\text{grad}}\mu_\gamma}{\overrightarrow{\text{grad}}T} \Leftrightarrow a = \alpha. \tag{3}$$

Thereby, the fit of the gradients plot gives the Seebeck coefficient at the given incident photon flux. Repeating this work 16 times at each different incident photon flux gives the variation of the Seebeck coefficient according to the incident illumination, as shown Fig. 3(b).

The Sackur-Tetrode expression for the entropy per particle of a monatomic gas of N particles is written as

$$\frac{S^\circ}{N} = k_B \ln\left[\frac{V}{N}\left(\frac{U}{N}\right)^{3/2}\right] + \frac{3}{2}k_B\left[\frac{5}{3} + \ln\left(\frac{4\pi m}{3h^2}\right)\right],$$

where V is the volume of the gas, U the internal energy of the gas, m the mass of one gas particle, and h Planck's constant.

The density of carriers at ambient temperature is written as

$$\frac{N}{V} = \frac{1}{4}\left(\frac{2m^{e,h}}{\pi\hbar^2}\right)^{3/2}(k_B T)^{3/2}\exp\left(-\frac{E_G}{2k_B T}\right),$$

with m^e, m^h the effective masses of electrons and heavy holes in the material (0.069 m_0 and 0.47 m_0, respectively).

The internal energy per particle of the monatomic gas is written as

$$\frac{U}{N} = E_G + \frac{3}{2} k_B T.$$

T is taken at 300 K for the computations.

IV. RESULTS AND DISCUSSION

At a given incident photon flux, from the photoluminescence data shown Fig. 2(a) (in this figure the photoluminescence intensity has been integrated in each pixel over all recorded wavelengths) it is possible to fit the spectrum of each pixel [Fig. 2(b) shows three spectra at different incident photon fluxes measured at the point at (94.1 μm; 70.0 μm); the linear fit is done between 0.81 and 0.86 eV]. According to Eq. (1), we therefore access the electrochemical potential and temperature map [see Figs. 2(c) and 2(d)]. The spatial variations of the observed electrochemical potentials and temperature are due to the diffusion of carriers in a permanent regime under local illumination [40,41].

The plot of this spatial electrochemical difference vs that of the temperature is shown in Fig. 3(a). We found a linear relationship between the two quantities, which is the Seebeck coefficient α of the material. Thereby, the slope gives the Seebeck coefficient at a given incident photon flux.

This result is experimental evidence of the micrometer-scale linear relationship between the temperature and electrochemical potential gradients.

Repeating this work 16 times at each different incident photon flux gives the variation of the Seebeck coefficient according to the incident illumination, as shown Fig. 3(b). In the studied intrinsic sample, the incident photon flux exceeds the rate of intrinsic carriers, so that the variation of the Seebeck coefficient depends only on the incident photon flux.

This observation of a thermopower in an intrinsic material is in agreement with Gurevich's work about the nature of thermopower in bipolar semiconducting materials [42]. The obtained values are at the same magnitude as *ab initio* computational modeling on this kind of structure [43].

By considering the Seebeck coefficient as an entropy per carrier, the Seebeck coefficient can be seen as

$$\alpha = \frac{k_B}{q} \ln(\phi_{\text{inc}}) - \frac{k_B}{q} \ln(\phi_{\text{BB}}) - \frac{1}{q} S^{\circ}, \tag{4}$$

where q is the absolute value of the elementary charge, ϕ_{inc} the incident photon flux, ϕ_{BB} the black body flux at ambient temperature, that is, the incident photon flux without light illumination, and S° the entropy per carrier at ambient temperature. With this simple model, the Seebeck coefficient should be linear with the logarithm of the incident photon flux with a slope of $(k_B/q) = 8.617 \times 10^{-5}$ eV K^{-1}. The fit performed on the experimental data and shown Fig. 3(b) exhibits a slope of 8.7223×10^{-5} eV K^{-1}, which is in good agreement with the theoretical prediction: the error is about 1.2%. This result is also in agreement with the linear decrease of the Seebeck coefficient with the logarithm of the carrier

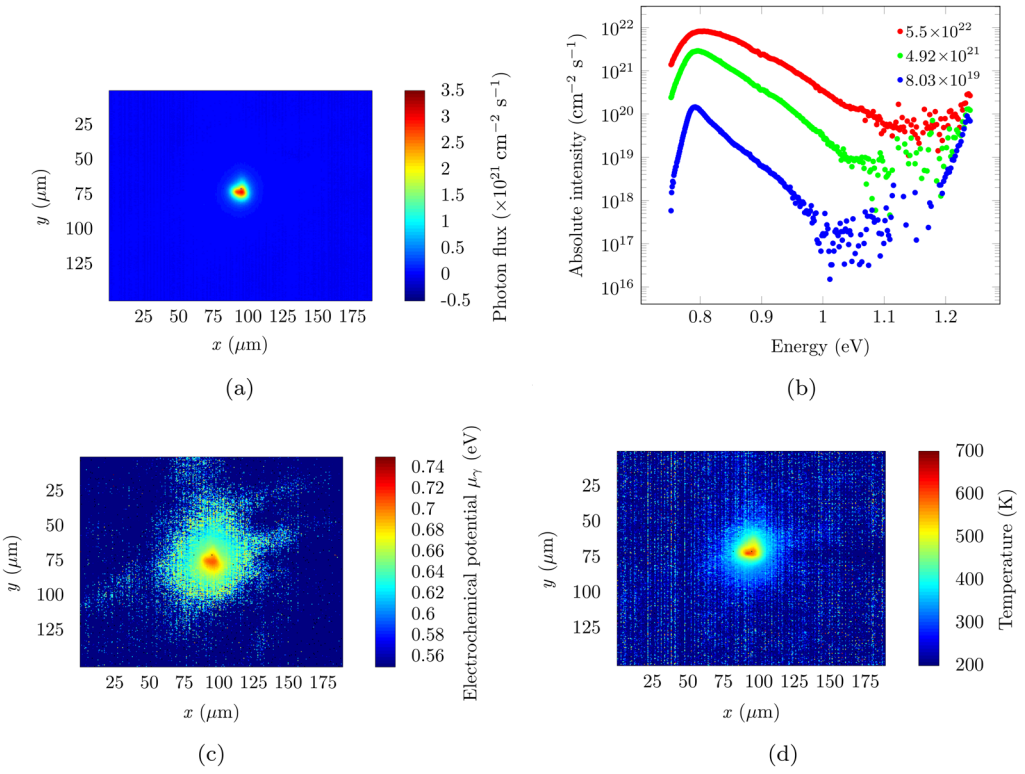

FIG. 2. Absolutely calibrated photoluminescence data and extracted thermodynamical parameters for one incident photon flux. (a) Integrated photoluminescence intensity map m^{-2} s^{-1}. (b) Absolutely calibrated photoluminescence spectra at the same point on the map for three different incident photon fluxes (5.05×10^{22} in red at the top, 4.92×10^{21} in green in the middle, 8.03×10^{19} in blue at the bottom, cm^{-2} s^{-1}). The high-energy tail variation is mainly due to carrier temperature variation. (c) Carrier electrochemical potential map (eV). (d) Carrier temperature map (K); the temperature decreases with the distance from the spot of the laser beam.

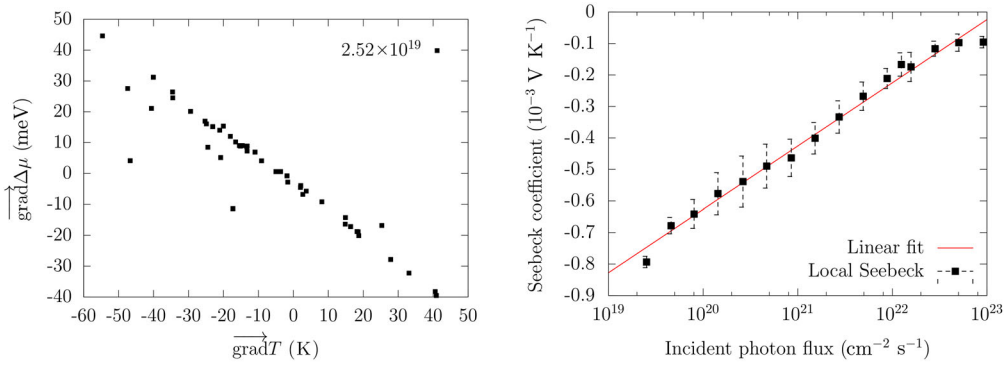

(a) (b)

FIG. 3. Linear Seebeck coefficient validity at micrometer scale and Seebeck coefficient linear variation with the incident photon flux. (a) Difference between two close pixels of the electrochemical potential map against the difference between the same pixels taken on the temperature map (incident photon flux of 2.52×10^{19}). This linear relationship shows that the slope can be considered as a linear Seebeck coefficient at micrometer scale. (b) Linear variation of the local Seebeck coefficient with the incident photon flux. Error bars are displayed in dashed vertical lines. The slope is 8.7723×10^{-5} eV K^{-1} and the intercept is $-0.004\,64$ V K^{-1} from the linear fit.

density called phenomenological Seebeck coefficient [44]. This linear decrease has also been observed in photo-Seebeck experiments, in which the Seebeck coefficient is measured while a light intensity modifies the carrier density [13–15].

Moreover, the slope appears to be disconnected with the material properties: indeed, the incident photon flux is independent from the material properties as well as k_B/q. The material-dependent quantity is given by the intercept C' in Eq. (4). From the linear fit of the Seebeck coefficient with the incident photon flux, $C' = -0.004\,643$ V K^{-1}. This intercept is obtained when $\phi_{\mathrm{inc}} = \phi_{\mathrm{BB}}$ and enables us to access to the entropy per carrier of the material at ambient temperature as

$$C' = -\frac{1}{q} S^{\circ}.$$

$S^{\circ} = 7.4 \times 10^{-22}$ J K^{-1} carrier^{-1}, which is 1.4 times more than the value given by the Sackur-Tetrode [45] expression, when summing the electron and hole contributions: $S^{\circ} = 5.4 \times 10^{-22}$ J K^{-1} carrier^{-1}. The difference between the Sackur-Tetrode value and the experimental one may come from the entropy of the lattice. Indeed, the Sackur-Tetrode expression is true for a monatomic gas; the fitted value corresponds to the entropy of the semiconducting material, carrier plasma, and lattice, divided by the number of electron-hole pairs. Finally, the contribution of the lattice of the material is more important than that of the carriers to the Seebeck coefficient: the material properties are closely related to the lattice, so that the intercept is the relevant quantity to compare different materials. The slope of the Seebeck coefficient with the incident photon flux does not depend on the material properties, but only on the carrier density.

V. CONCLUSION

The photoluminescence hyperspectral imaging has given the possibility to demonstrate the linear relationship between the temperature and electrochemical potential gradients at micrometer scale. This purely light-induced thermopower has been characterized by an optical contactless technique. The variation of the Seebeck coefficient with the carrier density is in good agreement with the theory. We also showed that the variation of the thermopower with the incident photon flux gives an access to the entropy per carrier in the material at an ambient temperature. These are useful quantities for characterizing the carrier populations in the semiconducting materials.

This Seebeck measurement technique facilitates the material research and the fundamental comprehension of the thermopower in the thermoelectric community, as we do not have to deal with material or electrical artifacts.

ACKNOWLEDGMENTS

F. G. acknowledges the French Ministry of Environment, Sustainable Development and Energy, for a grant. The Laboratory Foton INSA in Rennes (France) is acknowledged for providing the multi-quantum-well structure, and the C. Goupil (LIED laboratory, Paris) for fruitful discussions. Part of this work was performed in the framework of the program "New concepts in photovotaics" at IPVF under Contract No. ANR-IPVF-02.

[1] Thomas Johann Seebeck, Ueber die magnetische polarisation der metalle und erze durch temperaturdifferenz, Ann. Phys. (Berlin) **82**, 253 (1826).

[2] Shiho Iwanaga, Eric S. Toberer, Aaron LaLonde, and G. Jeffrey Snyder, A high-temperature apparatus for

measurement of the Seebeck coefficient, Rev. Sci. Instrum. **82**, 063905 (2011).
[3] C. Wood, A. Chmielewski, and D. Zoltan, Measurement of Seebeck coefficient using a large thermal gradient, Rev. Sci. Instrum. **59**, 951 (1988).
[4] M. Trakalo, C. J. Moore, J. D. Leslie, and D. E. Brodie, Apparatus for measuring Seebeck coefficients of high-resistance semiconducting films, Rev. Sci. Instrum. **55**, 754 (1984).
[5] Jonathan R. Widawsky, Pierre Darancet, Jeffrey B. Neaton, and Latha Venkataraman, Simultaneous determination of conductance and thermopower of single molecule junctions, Nano Lett. **12**, 354 (2012).
[6] K. P. Pernstich, B. Rössner, and B. Batlogg, Field-effect-modulated Seebeck coefficient in organic semiconductors, Nat. Mater. **7**, 321 (2008).
[7] B. Yang, J. L. Liu, K. L. Wang, and G. Chen, Simultaneous measurements of Seebeck coefficient and thermal conductivity across superlattice, Appl. Phys. Lett. **80**, 1758 (2002).
[8] N. Mateeva, H. Niculescu, J. Schlenoff, and L. R. Testardi, Correlation of Seebeck coefficient and electric conductivity in polyaniline and polypyrrole, J. Appl. Phys. **83**, 3111 (1998).
[9] H. J. Goldsmid and J. W. Sharp, Estimation of the thermal band gap of a semiconductor from Seebeck measurements, J. Electron. Mater. **28**, 869 (1999).
[10] F. G. Bass and Yu G. Gurevich, Thermomagnetic effects in an electron gas of semiconductors heated by a high-frequency electric field, Sov. Phys. JETP **25**, 112 (1967).
[11] Yu G. Gurevich and O. L. Mashkevich, Theory of thermoelectric effects in ambipolar semiconductors, Sov. Phys. Semicond. **24**, 835 (1990).
[12] Jan Tauc, The thermal photo-electric phenomenon in semiconductors, Chekh. Fiz. Zh. **5**, 528 (1955).
[13] P. S. Mondal, R. Okazaki, H. Taniguchi, and I. Terasaki, Photo-Seebeck effect in tetragonal PbO single crystals, J. Appl. Phys. **114**, 173710 (2013).
[14] Ryuji Okazaki, Ayaka Horikawa, Yukio Yasui, and Ichiro Terasaki, Photo-Seebeck effect in ZnO, J. Phys. Soc. Jpn. **81**, 114722 (2012).
[15] P. S. Mondal, R. Okazaki, H. Taniguchi, and I. Terasaki, Photo-transport properties of Pb_2CrO_5 single crystals, J. Appl. Phys. **116**, 193706 (2014).
[16] James G. Harper, Herman E. Matthews, and Richard H. Bube, Photothermoelectric effects in semiconductors: *n*- and *p*-type silicon, J. Appl. Phys. **41**, 765 (1970).
[17] Harry B. Kwok and Richard H. Bube, Thermoelectric and photothermoelectric effects in semiconductors: CdS single crystals, J. Appl. Phys. **44**, 138 (1973).
[18] F. L. Weichman, R. K. Lomnes, and S. Zukotynski, Photothermoelectric effects in CdS, Phys. Status Solidi (b) **25**, 583 (1968).
[19] Tristan DeBorde, Lee Aspitarte, Tal Sharf, Joshua W. Kevek, and Ethan D. Minot, Photothermoelectric effect in suspended semiconducting carbon nanotubes, ACS Nano **8**, 216 (2014).
[20] Eijiro Miyako, Chie Hosokawa, Masami Kojima, Masako Yudasaka, Ryoji Funahashi, Isao Oishi, Yoshihisa Hagihara, Mototada Shichiri, Mizuki Takashima, Keiko Nishio, and Yasukazu Yoshida, A photo-thermal-electrical converter based on carbon nanotubes for bioelectronic applications, Angew. Chem. **123**, 12474 (2011).
[21] Michele Buscema, Maria Barkelid, Val Zwiller, Herre S. J. van der Zant, Gary A. Steele, and Andres Castellanos-Gomez, Large and tunable photothermoelectric effect in single-layer MoS_2, Nano Lett. **13**, 358 (2013).
[22] Xiaodong Xu, Nathaniel M. Gabor, Jonathan S. Alden, Arend M. van der Zande, and Paul L. McEuen, Photothermoelectric effect at a graphene interface junction, Nano Lett. **10**, 562 (2010).
[23] James G. Harper, Two-carrier photothermoelectric effects in GaAs, J. Appl. Phys. **41**, 3182 (1970).
[24] Dirk König, Daniel Hiller, Margit Zacharias, Stephan Michard, and Christopher Flynn, Static hot carrier populations as a function of optical excitation energy detected through energy selective contacts by optically assisted IV excitation energy, Prog. Photovoltaics **22**, 1070 (2014).
[25] G. J. Conibeer, D. König, M. A. Green, and J. F. Guillemoles, Slowing of carrier cooling in hot carrier solar cells, Thin Solid Films **516**, 6948 (2008).
[26] Antonio Luque and Antonio Martí, Electronphonon energy transfer in hot-carrier solar cells, Sol. Energy Mater. Sol. Cells **94**, 287 (2010).
[27] Y. Rosenwaks, M. C. Hanna, D. H. Levi, D. M. Szmyd, R. K. Ahrenkiel, and A. J. Nozik, Hot-carrier cooling in GaAs: Quantum wells versus bulk, Phys. Rev. B **48**, 14675 (1993).
[28] Gordon Lasher and Frank Stern, Spontaneous and stimulated recombination radiation in semiconductors, Phys. Rev. **133**, A553 (1964).
[29] P. Würfel, The chemical potential of radiation, J. Phys. C **15**, 3967 (1982).
[30] L. C. Hirst, M. P. Lumb, R. Hoheisel, C. G. Bailey, S. P. Philipps, A. W. Bett, and R. J. Walters, Spectral sensitivity of hot carrier solar cells, Sol. Energy Mater. Sol. Cells **120**, 610 (2014).
[31] A. Le Bris, L. Lombez, S. Laribi, G. Boissier, P. Christol, and J.-F. Guillemoles, Thermalisation rate study of GaSb-based heterostructures by continuous wave photoluminescence and their potential as hot carrier solar cell absorbers, Energy Environ. Sci. **5**, 6225 (2012).
[32] S. A. Lyon, Spectroscopy of hot carriers in semiconductors, J. Lumin. **35**, 121 (1986).
[33] Amaury Delamarre, Laurent Lombez, and Jean-François Guillemoles, Characterization of solar cells using electroluminescence and photoluminescence hyperspectral images, J. Photon. Energy **2**, 027004 (2012).
[34] R. V. Forest, E. Eser, B. E. McCandless, J. G. Chen, and R. W. Birkmire, Effect of Na on Cu(In,Ga)Se2 in-plane conductance and Seebeck coefficient, in *Proceedings of the IEEE 40th Photovoltaic Specialist Conference (PVSC), 2014* (IEEE, New York, 2014), pp. 0345–0349.
[35] Gehong Zeng, Joshua M. O. Zide, Woochul Kim, John E. Bowers, Arthur C. Gossard, Zhixi Bian, Yan Zhang, Ali Shakouri, Suzanne L. Singer, and Arun Majumdar, Cross-plane Seebeck coefficient of ErAs: InGaAs/InGaAlAs superlattices, J. Appl. Phys. **101**, 034502 (2007).
[36] Daryoosh Vashaee, Yan Zhang, Ali Shakouri, Gehong Zeng, and Yi-Jen Chiu, Cross-plane Seebeck coefficient in superlattice structures in the miniband conduction regime, Phys. Rev. B **74**, 195315 (2006).

[37] Yan Zhang, Gehang Zeng, Rajeev Singh, J. Christofferson, Edward Croke, J. E. Bowers, and Ali Shakouri, Measurement of Seebeck coefficient perpendicular to SiGe superlattice, in *Proceedings of ICT'02: The Twenty-First International Conference on Thermoelectrics, 2002* (IEEE, 2002), pp. 329–332.

[38] J. M. O. Zide, D. Vashaee, Z. X. Bian, G. Zeng, J. E. Bowers, A. Shakouri, and A. C. Gossard, Demonstration of electron filtering to increase the Seebeck coefficient in $In_{0.53}Ga_{0.47}As/In_{0.53}Ga_{0.28}Al_{0.19}As$ superlattices, Phys. Rev. B **74**, 205335 (2006).

[39] Amaury Delamarre, Laurent Lombez, and Jean-François Guillemoles, Contactless mapping of saturation currents of solar cells by photoluminescence, Appl. Phys. Lett. **100**, 131108 (2012).

[40] D. Paget, F. Cadiz, A. C. H. Rowe, F. Moreau, S. Arscott, and E. Peytavit, Imaging ambipolar diffusion of photocarriers in GaAs thin films, J. Appl. Phys. **111**, 123720 (2012).

[41] F. Cadiz, D. Paget, A. C. H. Rowe, T. Amand, P. Barate, and S. Arscott, Effect of the Pauli principle on photoelectron spin transport in p^+ GaAs, Phys. Rev. B **91**, 165203 (2015).

[42] Yu. G. Gurevich, O. Yu. Titov, G. N. Logvinov, and O. I. Lyubimov, Nature of the thermopower in bipolar semiconductors, Phys. Rev. B **51**, 6999 (1995).

[43] Mona Zebarjadi, Ali Shakouri, and Keivan Esfarjani, Thermoelectric transport perpendicular to thin-film heterostructures calculated using the Monte Carlo technique, Phys. Rev. B **74**, 195331 (2006).

[44] Jianwei Cai and G. D. Mahan, Effective Seebeck coefficient for semiconductors, Phys. Rev. B **74**, 075201 (2006).

[45] H. von Tetrode, Die chemische konstante der gase und das elementare wirkungsquantum, Ann. Phys. (Berlin) **343**, 434 (1912).